International Forum on Aeroelasticity and Structural Dynamics
IFASD 2022
13-17 June 2022, Madrid, Spain

GUST AND MANOUVRE LOADS ALLEVIATION TECHNOLOGIES: OVERVIEW, RESULTS AND LESSON LEARNED IN THE FRAMEWORK OF THE CS2 AIRGREEN2 PROJECT

Francesco Toffol[1], Luca Marchetti[1], Sergio Ricci[1], Federico Fonte[1*], Elisa Capello[2] and Simone Malisani[2]

[1] Politecnico di Milano, Department of Aerospace Sience and Technology
Via La Masa 34, 20156, Milano, Italy
francesco.toffol@polimi.it
luca.marchetti@polimi.it
sergio.ricci@polimi.it
federico.fonte@polimi.it
*Currently Rotor Dynamics, Leonardo Helicopter Division, 21017, Cascina Costa, Italy

[2] Politecnico di Torino, Department of Mechanical and Aerospace Engineering
Corso Duca degli Abruzzi 24, 10129, Torino
elisa.capello@polito.it
simone.malisani@polito.it

Keywords: active control, Gust and Maneuver load alleviation, robust control systems

Abstract: This paper provides the description of the design, validation and testing of devices and active control laws for the alleviation of dynamic loads on a new generation regional aircraft. The main objective of the designed control laws is the alleviation of wing loads due to discrete gusts and maneuvers. The first part of this paper introduces the project and the framework in which it was developed. Then a description of the numerical models is provided, together with the design methodologies of the active controllers.
Finally, the results of an aero-servo-elastic wind tunnel test campaign are compared with the numerical simulation.

1. INTRODUCTION

Dynamic loads have an important role in the wing load sizing envelope, and they may result one of the most critical conditions, moreover they affect the fatigue of the wing components. The active load control helps to reduce the magnitude of these loads and can lead to structural improvement as shown in the ’50 by the Bristol Brabazon, that was designed with a structure 20% weaker than necessary thanks to the designer faith in the Gust Load Alleviation (GLA) feed-forward controller [1]. More recently, a Nasa Technical Memorandum [2] provided an historical survey of the active control technique used in many commercial and military aircraft. Early GLA attempts faced the problem considering the rigid aircraft [3][4], but with the design of new flexible aircraft the problem became aero-elastic and modal control started to appear. The field of application, in the ’70, was restricted to the military vehicles like the XB-70 [5][6] and B-52 [7], where the Load Alleviation and Mode Suppression (LAMS) used gyroscopic measures to drive the deflection of ailerons, rudder and elevator.

The Lockheed L-1011 represented one of the first application on a commercial aircraft, it was equipped with a controller moving the ailerons with feedback on accelerations measured in the wing tips and in the fuselage [8].
Most applications of alleviation control laws exploited the conventional control surfaces, but in some cases dedicated devices were developed, for example the GLAS on the B-2 Spirit [9].
Another application of dedicated control surfaces for aeroelastic mode control appeared with the B-1 Lancer [2], where dedicated nose mounted, small tabs were used to damp the fuselage bending mode. Nowadays, all the commercial aircraft are equipped with some kind of load alleviation system [2].
Wind tunnel tests helps to validate the numerical models in a controlled environment, reproducing the desired 1-cos gust shape. Indeed, during flight test it is almost impossible to encounter a 1-cos gust with prescribed amplitude and gust repeatability is even rarer. Moreover, wind tunnel testing is cheaper and safer with respect to flight test.
Some alleviation tests were performed flying an aircraft into its own wake or in the wake of another aircraft [10][11], but it is almost impossible to reproduce the most critical gust.
Wind tunnel is a controlled environment where the test can be performed using scaled models that mimic the behavior of the reference aircraft. These are aero-servo-elastic models equipped with movable control surfaces and different control laws can be applied to compare their effectiveness. Some examples of aero-servo-elastic actively controlled models can be found in [12]-[31].

2. THE CLEAN SKY 2 AIRGREEN2 PROJECT

The Clean Sky 2 AIRGREEN2 project [32] aims to develop a more efficient wing studying innovative devices [33] to improve the aero-structural efficiency and aero-acoustic footprint of a new generation regional aircraft.
The AIRGREEN2 consortium is composed by many industrial partners, research institutions and universities, creating a fertile environment where developing new concepts. The project aims to increase the technology readiness level of the future regional aircraft by increasing the overall technology readiness level and testing some of them in flight by the end of 2022.
The device developed in this framework are mainly four and all of them modify the wing shape to achieve benefits in terms of aerodynamic performances or load alleviation capabilities. The developed devices are:

- A morphing Droop Nose (DN) in substitution of conventional slats, which ensures better take-off and landing performances reducing the noise and increasing the efficiency [34]-[39] also allowing at the same time the adoption of natural laminar wings due to thanks to the gapless solution.
- A morphing flap, that is used in combination with the DN to improve the high-lift phases and the cruise performances when retracted, since its final part can be used as an additional small trailing edge surface [40] helping to implement load control technologies.
- A morphing winglet, equipped with two movable surfaces implementing the finger-like structure that improves the climb performances and can perform Maneuver Load Alleviation (MLA).
- An Innovative Wing Tip (IWT) device, used as an alternative to the winglet, that is designed to perform both Maneuver and Gust Load Alleviation (MLA/GLA) [41][42].

These devices were deeply studied and designed to reach a TRL 5. Finally, the Winglet and the IWT will be flight tested by the end of 2022 to provide a preliminary assessment of their load alleviation and performances improvement capabilities.

The project goal goes beyond the design and realization of the innovative device IWT, an important portion consists in the development of the active control laws that must be implemented on the real aircraft.
Within the project, intermediate experiments were realized to assess the effectiveness of the designed devices and of the control laws: the aerodynamic performances of the innovative wing were characterized with a 1:3 scaled model (WTT2) of the wing tested in a transonic wind tunnel; the alleviation capability of the IWT and the active control technologies were tested on a 1:6 aero-servo-elastic wind tunnel model (WTT3), while the flying prototypes of the innovative device IWT underwent to structural test to achieve the permit to flight.
Since the reference aircraft doesn't exist yet, the flying item were adapted to fit on a similar aircraft, i.e. the existing C-27J Spartan selected by Leonardo for the final flight test inside CS2 program.

3. SIMULATION MODEL

The reference regional aircraft for the project is a Turboprop designed to accommodate 90 passengers and it is shown in Figure 1.

Figure 1: Artistic rendering of the Leonardo's TP90

The reference numerical model of TP90 for the aeroelastic simulation carried out during the entire AIRGREEN2 project is represented by a stick model where the structure is represented by beam elements and the aerodynamics is modelled with a doublet-lattice (DLM) or vortex-lattice (VLM) method depending on the required analysis. Several payload and fuel configurations can be simulated using different sets of concentrated masses. This kind of representation of the aircraft is widely used for the computation of the load envelopes because it combines the ideal trade-off between model's complexity and fidelity.

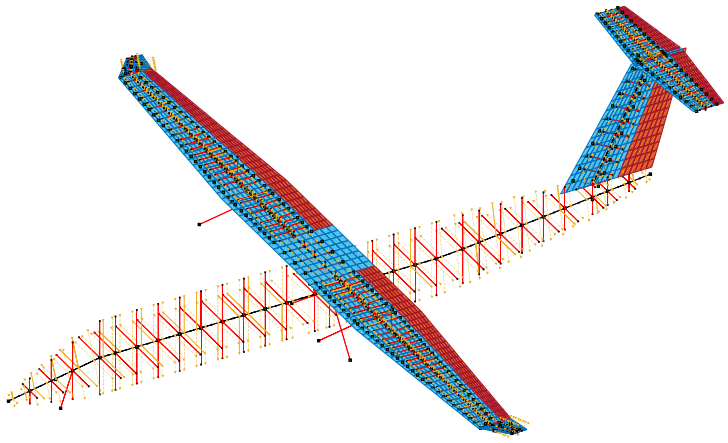

Figure 2: TP90's aeroelastic stick model with the Innovative Wing Tip

The model is written in a standard NASTRAN format, which is also the standard input file for NeoCASS [44][45][46], which is the aero-servo-elastic design and analysis suite developed by Politecnico di Milano. The analyses presented in this work are performed with NeoCASS since it allows for an automatic transformation of the aeroelastic model into the corresponding State-Space (SS) model, which allows to develop control laws in time domain and allows to create complex Simulink model where the complete non-linear model of the actuator can be easily added.
The problem is projected on its modal basis, the State-Space model of the structural part is built with the modal mass, damping and stiffness matrices obtained as in Eq.(1), where $\boldsymbol{U}$ is the eigenvector matrix, the subscripts *gg* indicates global matrices and *hh* modal ones.

$$\begin{aligned}
\mathbf{M_{hh}} &= \mathrm{U}^{\mathrm{T}} M_{gg} U = \begin{bmatrix} \ddots & & \\ & \mathrm{m_i} & \\ & & \ddots \end{bmatrix} \\
\mathbf{C_{hh}} &= \mathrm{U}^{\mathrm{T}} C_{gg} U = \begin{bmatrix} \ddots & & \\ & c_{\mathrm{i}} & \\ & & \ddots \end{bmatrix} \\
\mathbf{K_{hh}} &= \mathrm{U}^{\mathrm{T}} K_{gg} U = \begin{bmatrix} \ddots & & \\ & \mathrm{k_i} & \\ & & \ddots \end{bmatrix}
\end{aligned} \tag{1}$$

The DLM provides the computation of a transfer function, evaluated for a given set of reduced frequencies and Mach numbers, where the output is a generalized modal forces and the input can be the structural motion, the gust amplitude or an imposed motion of the aerodynamic mesh e.g. one or multiple control surfaces, leading to an expression of the Generalized Aerodynamic Forces (GAFs) as in Eq.(2).

$$\boldsymbol{GAFs} = q_\infty(\boldsymbol{H_{am}}(k, Ma)\boldsymbol{q} + \boldsymbol{H_{ag}}(k, Ma)v_g + \boldsymbol{H_{au}}(k, Ma)\boldsymbol{u}) \tag{2}$$

To obtain the State-Space representation of the aero-servo-elastic system, the GAFs must be translated into the time domain. This is done using the Matrix Fraction Approximation (MFA) algorithm implemented in NeoCASS and described in [43]. Starting from the identification of the $\boldsymbol{H_{am}}$ term, the one due to the structural motion, the transfer function is approximated to obtain a State-Space system in the form of Eq.(5), where the input is the structural motion and the output are the aerodynamic forces projected on the modal base.

$$\begin{cases} \dot{\mathbf{x}}_a &= \mathbf{A}\mathbf{x_a} + \mathbf{B}\mathbf{q} \\ \boldsymbol{Q_a} &= \mathbf{C}\mathbf{x_a} + \mathbf{D}\mathbf{q} \end{cases} \tag{3}$$

The MFA approximates the aerodynamic transfer function as in Eq.(4) by computing the $\boldsymbol{A_a}, \boldsymbol{B_a^i}, \boldsymbol{C_a}, \boldsymbol{D_a^i}$ matrices. $p = \sigma + jk$ is the normalized Laplace variable.

$$\mathbf{H}_{am}(p) \approx \mathbf{D^0}_a + p\mathbf{D^1}_a + p^2\mathbf{D^2}_a + \mathbf{C}_a(p\mathbf{I} - \mathbf{A}_a)^{-1}\left(\mathbf{B^0}_a + p\mathbf{B^1}_a + p^2\mathbf{B^2}_a\right) \tag{4}$$

The identified matrices are used to assemble the dynamic SS-model that represents the aerodynamic system, having the modal coordinates as input and the generalized aerodynamic forces as output.

$$\begin{cases} \dfrac{d\mathbf{x}_a}{dt} &= \dfrac{1}{t_a}\mathbf{A}_a\mathbf{x}_a + \dfrac{1}{t_a}\mathbf{B^0}_a\mathbf{q} + \mathbf{B^1}_a\dot{\mathbf{q}} + t_a\mathbf{B^2}_a\ddot{\mathbf{q}} \\ \mathbf{Q_a} &= \mathbf{C}_a\mathbf{x}_a + \mathbf{D^0}_a\mathbf{q} + t_a\mathbf{D^1}_a\dot{\mathbf{q}} + t_a^2\mathbf{D^2}_a\ddot{\mathbf{q}} \end{cases} \tag{5}$$

The SS-system of Eq.(5) is coupled to the mechanical SS-model, providing the coupling between the elastic and aerodynamic system and creating the full aero-elastic system in time domain, as described in Eq. (6).

$$\begin{bmatrix} \mathbf{I} & \mathbf{0} & \mathbf{0} \\ \mathbf{0} & \mathbf{M} - q_\infty t_a^2 \mathbf{D^2}_a & \mathbf{0} \\ \mathbf{0} & -t_a^2 \mathbf{B^2}_a & t_a \mathbf{I} \end{bmatrix} \frac{d}{dt} \begin{bmatrix} \mathbf{q} \\ \dot{\mathbf{q}} \\ \mathbf{x}_a \end{bmatrix} = \begin{bmatrix} \mathbf{0} & \mathbf{I} & \mathbf{0} \\ -(\mathbf{K} - q_\infty \mathbf{D^0}_a) & -(\mathbf{C} - q_\infty t_a \mathbf{D^1}_a) & q_\infty \mathbf{C}_a \\ \mathbf{B^0}_a & t_a \mathbf{B^1}_a & \mathbf{A}_a \end{bmatrix} \begin{bmatrix} \mathbf{q} \\ \dot{\mathbf{q}} \\ \mathbf{x}_a \end{bmatrix} \tag{6}$$

The same approach is used to identify the forces due to the gust (Eqs. (4)(5)), leading to the aeroelastic system of Eq.(7) where the subscript a+g indicates the modal + gust contribution and the subscript ag indicates the only gust contribution.

$$\begin{bmatrix} \mathbf{I} & \mathbf{0} & \mathbf{0} \\ \mathbf{0} & \mathbf{M} - q_\infty t_a^2 \mathbf{D^2}_a & \mathbf{0} \\ \mathbf{0} & -t_a^2 \mathbf{B^2}_a & t_a \mathbf{I} \end{bmatrix} \frac{d}{dt} \begin{bmatrix} \mathbf{q} \\ \dot{\mathbf{q}} \\ \mathbf{x}_a \end{bmatrix} =$$

$$+ \begin{bmatrix} \mathbf{0} & \mathbf{I} & \mathbf{0} \\ -(\mathbf{K} - q_\infty \mathbf{D^0}_a) & -(\mathbf{C} - q_\infty t_a \mathbf{D^1}_a) & q_\infty \mathbf{C}_{a+g} \\ \mathbf{B^0}_a & t_a \mathbf{B^1}_a & \mathbf{A}_{a+g} \end{bmatrix} \begin{bmatrix} \mathbf{q} \\ \dot{\mathbf{q}} \\ \mathbf{x}_{a+g} \end{bmatrix} \tag{7}$$

$$+ \frac{1}{V_\infty} \begin{bmatrix} \mathbf{0} & \mathbf{0} & \mathbf{0} \\ q_\infty \mathbf{D^0}_{ag} & q_\infty t_a \mathbf{D^1}_{ag} & q_\infty t_a^2 \mathbf{D^2}_{ag} \\ \mathbf{B^0}_{ag} & t_a \mathbf{B^1}_{ag} & t_a^2 \mathbf{B^2}_{ag} \end{bmatrix} \begin{bmatrix} \mathrm{v}_g \\ \dot{v}_g \\ \ddot{v}_g \end{bmatrix}$$

where:

$$\mathrm{A}_{a+g} = \begin{bmatrix} A_a & \\ & A_{ag} \end{bmatrix}; C_{a+g} = [C_a \quad C_{ag}]; x_{a+g} = \begin{bmatrix} x_a \\ x_{ag} \end{bmatrix} \tag{8}$$

This leads to the aeroelastic system of Eq.(9), where $\boldsymbol{u_g}$ is the forcing term due to the gust and its derivatives up to the second order.

$$\begin{cases} \dot{\mathbf{x}}_{ae} & = \mathbf{A_{ae}} \mathbf{x_{ae}} + \mathbf{B_{ae}} \boldsymbol{u_g} \\ \boldsymbol{y} & = \mathbf{C_{ae}} \mathbf{x_{ae}} + \mathbf{D_{ae}} \mathbf{u_g} \end{cases} \tag{9}$$

Finally, the full aero-servo-elastic State Space model becomes:

$$\begin{cases} \dot{\boldsymbol{x}} & = \mathbf{A}\mathbf{x} + \mathbf{B_u}\mathbf{u} + \mathbf{B_g}\boldsymbol{g} \\ \boldsymbol{y} & = \mathbf{C}\mathbf{x} + \mathbf{D_u}\mathbf{u} + \mathbf{B_g}\boldsymbol{g} \end{cases} \tag{10}$$

where the control input $\boldsymbol{u}$ contribution is accounted as well.
A State-Space representation of the aeroelastic system such as the one in Eq.(10) is entirely defined in time domain and can be used to simulate dynamic analysis using an integration method or to develop control laws using design methodologies in time domain.
It was realized a SS model of each mass configuration and, since the aerodynamic matrices dependency with respect to the Mach number, for each flight point.

The aero-servo-elastic SS model can be easily implemented in a Simulink model, which allows to add external blocks to simulate sensors, actuators, and acquisition parameters, providing a high-fidelity dynamic simulator of the reference aircraft. In particular, the detailed Simulink model of the IWT's control surface actuator was provided by Umbra, the company in charge of its development and manufacturing, and it was added to the model: it transforms the commanded position coming from the top level GLA controller into the real surface rotation considering the non-linear kinematic of the actuation chain, the speed, stroke and force saturations of the actuator and the full control logic. Moreover, the discrete time implementation of the Simulink model allows to reproduce the sampling rates available on the aircraft and the Flight Control Computer (FCC) performances, its simplified scheme is represented in Figure 3.

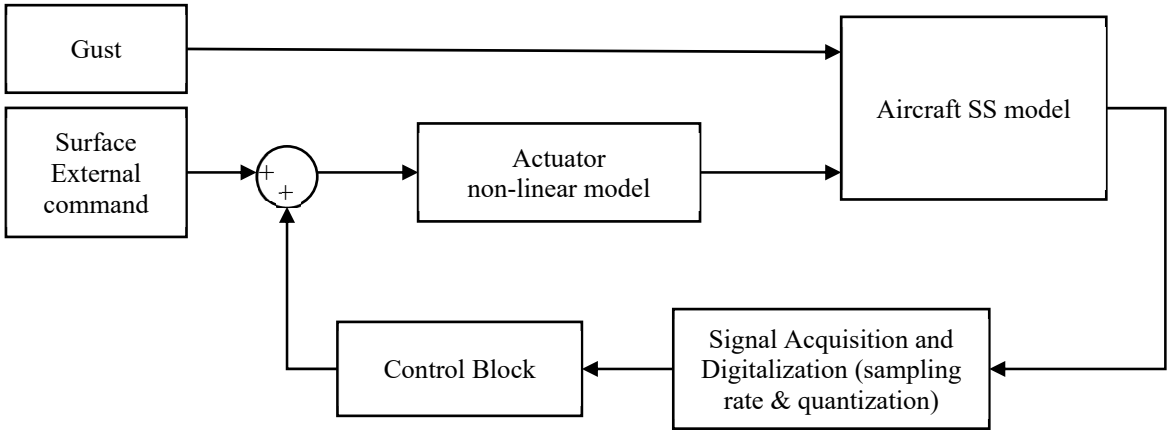

Figure 3: Aero-servo-elastic Simulink model of the TP90

4. CONTROL LAWS DESIGN

The responsibility of design of active aeroelastic control was in charge of Politecnico di Milano (POLIMI), with the contribution of Politecnico di Torino (POLITO). One of the requirements of the project was the implementation of a GLA controller able to achieve a 20% reduction of the wing root bending moment, using all the available control surfaces, and taking into account the actual performances of the actuation system. Specifically, POLIMI and POLITO proposed two different controller's structure, respectively: the first one is a Static Output Feedback controller while the second one is an H_∞ robust controller. Both the approaches are described in the following.

4.1. STATIC OUTPUT FEEDBACK CONTROLLER

Static Output Feedback (SOF) controllers [47] are a class of controllers where the control input, $\boldsymbol{U}(s)$, is obtained as linear combination of the measured responses, $\boldsymbol{Y}(s)$, by means of a multiplication by a constant gain matrix, $\boldsymbol{G}$, as $\boldsymbol{U}(s) = \boldsymbol{G}\,\boldsymbol{Y}(s)$. The SOF approach has been successfully applied to synthetize aeroservoelastic controllers for gust load alleviation [50] and flutter suppression [48][49].

Once the control input and the measured responses are defined, the design of the controller is completed by the computation of the elements of the gain matrix $\boldsymbol{G}$. The approach used here to get the gain matrix relies on the minimization of a weighted H_2 norm of a properly defined closed loop system whose input is the set of expected disturbances on the system, and the output contains the set of system quantities whose response to the disturbance need to be minimized and that are called performance output [50]. For a gust load alleviation controller, for example, the disturbance input is represented by the gust velocity, while the performance output can include internal forces and moments in several locations on the structure. In addition to the performance output also the control input must be included in the computation of the H_2 norm, so to both obtain a well posed optimization problem and to limit the control action.

The minimization of the closed loop H_2 norm is equivalent to the minimization of a quadratic cost function associated with the norm of the control input $\boldsymbol{u}$ and performance output $\boldsymbol{z}$ [47][51], as described by Eq.(10):

$$J = \int_0^\infty [\boldsymbol{z}^T \boldsymbol{W}_{zz} \boldsymbol{z} + \boldsymbol{u}^T \boldsymbol{W}_{uu} \boldsymbol{u}] dt \tag{11}$$

The relative importance of the performance and control input in the computation of the cost function is defined through two weight matrices, namely $\boldsymbol{W_{zz}}$ and $\boldsymbol{W_{uu}}$, which represents an additional tuning parameter set used to adjust the controller behavior.

The optimization of the cost function associated with the SOF control, and then the computation of the gain matrix, need to be performed numerically since no closed form equation exists. In the present work the algorithm described in [50] is used to perform the numerical optimization. In this work, the measures available on the real aircraft are the acceleration of the wing tips and of the CoG, together with the aircraft pitch rate. The acceleration measures are integrated through a numerical integrator to obtain the velocities which are then used by the SOF controller as independent input measures.

In the design of the gust load alleviation controller all the available control surfaces are considered as control input: the ailerons, the IWTs movable flaps and the elevator. The disturbance used to define the H_2 norm is constituted by the gust input, which is associated to a shape filter to focus the action on the frequency range of interest. The performance output contains the bending and torsional moments measured at wing root and the rigid displacement and rotation of the whole aircraft; the latter is inserted to minimize the impact of the controller on the low-frequency rigid body response of the aircraft.

Figure 4 shows the SOF control block, the inputs are already digitalized, and the acceleration integrated through a discrete integrator to obtain the structural velocities, for a total of 7 input. Considering the most general implementation of the SOF, the outputs are the 6 independent control surfaces (2 IWTs flap, 2 ailerons, 1 elevator, 1 rudder). The rudder is considered for sake of generality and for eventual use for MLA purpose. The gain matrix becomes a 6x7 matrix, with a total of 42 elements to be defined. Through the selection of the inputs (full set or reduced), symmetry consideration (symmetric deflection for symmetric phenomena) and the decoupling between longitudinal and lateral dynamics, the number of unknowns can be drastically reduced.

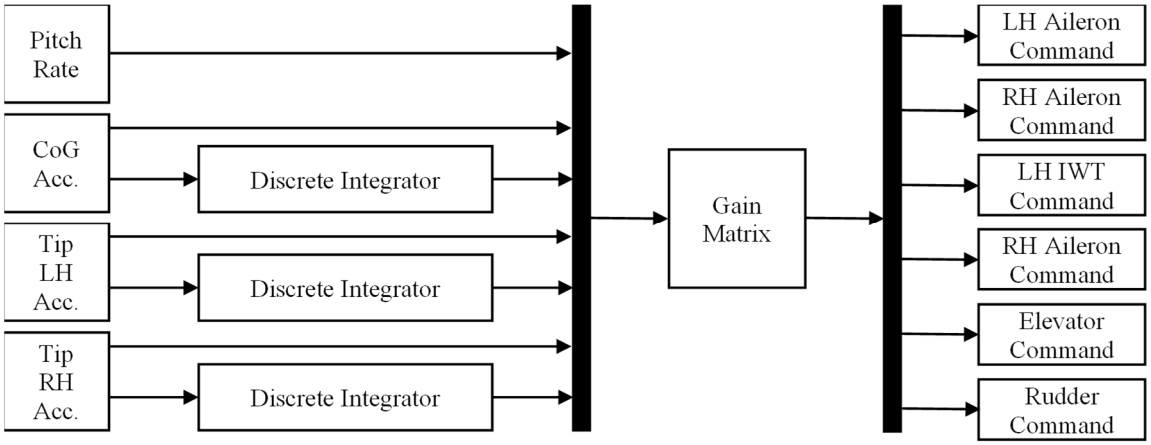

Figure 4: SOF scheme, also including the rudder command for eventual MLA purpose

With this approach, three different controllers were designed, and they are briefly described in the following.

- SOF401: it is a control law that exploits all the available control surfaces, i.e. aileron, elevator and IWT, it is focused on the WRBM reduction due to the gust. The feedback measures are the ones available (accelerations).
- SOF400: it is similar to the SOF401, but it uses only the IWT surface to assess the alleviation of the device in standalone operation. The feedback measures are the one available (accelerations).
- SOF003: it is the latest controller developed and it is oriented to the flight tests, it combines MLA and GLA capabilities of the IWT only and its objective is the reduction

of the WRBM without increasing the tip bending and torsional moment. This latest aspect is crucial because the device will be retro-fitted on an existing aircraft (C-27J) which wing structure is already sized for the design load of its baseline version. The feedback is represented by the pitch rate and the structural velocities obtained through the numerical integration of the accelerations, hence only 4 quantities.

Table 1: SOF controllers summary

Name	Aim	TP90 Configuration	Control surfaces used
SOF400	GLA	TP90-IWT	IWT only
SOF401	GLA	TP90-IWT	IWT + Aileron + Elevator
SOF003	GLA/MLA	TP90-IWT	IWT only

All the controllers are a single gain matrix designed to cover all the flight envelope and mass configurations, avoiding interpolation scheme or gain scheduling.

4.2. H∞ CONTROLLER

As robust control system an $\mathcal{H}_\infty$ optimal controller is proposed. Aim of the controller is to minimize the effect of the disturbances w_g (gust) and the performance output z, while guaranteeing internal stability of the closed-loop system.
The state-feedback $\mathcal{H}_\infty$ controller is combined with a state observer for a full state control system. The motivation for choosing a controller of such a simple form is twofold: i) we aim at obtaining a simple-enough controller, ii) output feedback $\mathcal{H}_\infty$cannot be coupled to the robust LMI techniques we want to apply, iii) this problem should be treated as a Multi-Input-Multi-Output (MIMO) system. The scheme of a classical state feedback controller is in Figure 5.

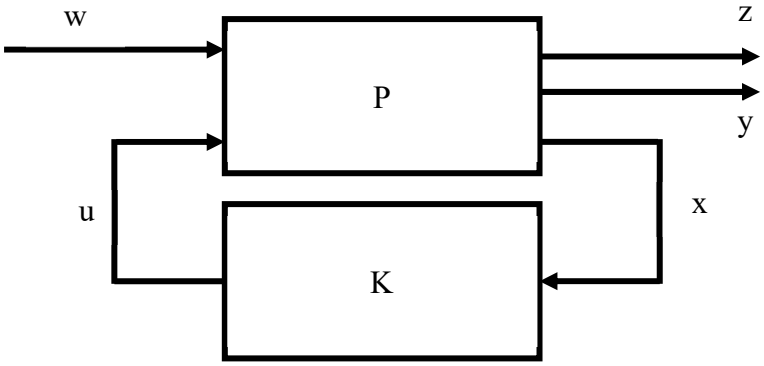

Figure 5: Classical scheme for $\mathcal{H}\infty$ controller

The first step is the definition of a classical state-feedback $\mathcal{H}_\infty$, using an LMI approach for the evaluation of the gain matrix. Starting from the theory presented in [52], the following LMIs has to be solved to find the gain matrix K

$$\begin{bmatrix} AQ + QA^T + B_uY + Y^TB_u^T & * & * \\ C_ZQ + D_{Zu}Y & -\gamma^2\mathbf{1} & * \\ B_w^T & D_{Zw}^T & * \end{bmatrix} < 0 \qquad (12)$$

where '*' indicates the symmetric terms of the matrix. A is the state matrix of the flexible system, C_Z is the matrix of output (i.e. the wing root loads), B_u and B_w are the control matrices related to the deflection surfaces and to the gust, respectively. The gain that must be reduced is γ. Q and Y are the unknown matrices to be evaluated, Q>0.
The matrix K of the control is the obtained as $K = YQ^{-1}$.

The controller we designed follows the scheme depicted in Figure 5 The control separates the rigid and the flexible modes. A classical LQR control is first designed to stabilize the rigid modes using only the elevator, and then a state-feedback $\mathcal{H}_\infty$ controller takes care of the flexible modes only, minimizing the $\mathcal{H}_\infty$ gain between w_g and z, using the aileron and the wing tip as control action.

For the definition of this controller, the actuator dynamics is included in the aircraft state-space model building a so-called augmented system. This means that a new state vector is created, which includes the plant state and the actuator one. In this way, the input u represents no more the actual command deflection, but it can be identified with the command required by the pilot or the control system. The command deflection is instead given by the actuator state (or output) vector components. An example of this kind of augmented system is given in [53], where the aircraft longitudinal dynamics state-space model is augmented with the elevator actuator dynamics.

Moreover, since in most practical cases the system states cannot be measured by direct observation, a state observer that provides an estimate of the states, exploiting measurements of the input and output of the real system, is designed. If a system is observable, the state observer allows the fully reconstruction of the system state from its output measurements [54].

Since the control command obtained with the design of an H∞ controller is too high, the minimum achievable gain is used as a metric by which a control-effector design is assessed, in which limitations on the aileron rate and deflection are considered in the design of the controller gain. Thus, a randomized H∞ controller is synthesized, considering an LMI approach for the definition of the feedback controller.

To analyze a more realistic case, the controller is synthesized starting from the measurements of on-board sensors, considering both IMU data (in terms of z, dz/dt, θ, q) and the wing accelerations in three selected sections.

Some remarks are at hand: a “unique” observer is designed for all the flight conditions. This is necessary since the observer design needs the knowledge of the system matrices. The choice of “nominal” matrices A, B is obvious; the gust disturbance does not contribute to the estimation process, since this signal is not measurable on board, being a disturbance.

5. NUMERICAL RESULTS

This section summarizes the results obtained with the numerical simulator for both the controller methodologies and the results are non-dimensional or the axes label intentionally omitted for confidentiality reasons.

The results are presented in terms of load envelope and the comparison is done with the open loop condition. The envelope is obtained with the Simulink model presented in Figure 3, testing 10 gusts with an equally spaced frequency, both positive and negative amplitude, between 1 and 10Hz, over 7 flight points and 6 mass configurations. The envelope is made of a total of 840 gust load cases for each controller. Figure 6 shows the monitoring sections spanwise used to evaluate the alleviation capabilities.

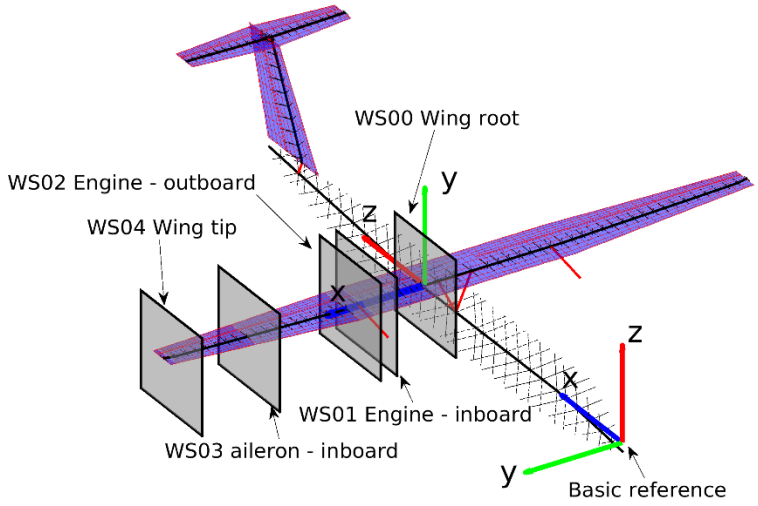

Figure 6: Monitoring sections spanwise

Figure 7 to Figure 9 show the open and close loop bending/torque envelopes obtained with the SOF controllers, which were normalized considering the maximum torque/bending values, directly obtaining the alleviation in term of % reduction. The most effective controller, in term of Wing Root Bending Moment (WRBM) reduction is the SOF401, the one that exploits all the movable surfaces of the aircraft. As, a drawback, this controller increases the torsional moment in some portions of the wing (mainly in the inner part). The SOF400 uses only the IWT control surfaces and reaches lower WRBM reduction, but the torsional moment increase is limited. The SOF003 controller, mainly oriented to the flight tests, has lower alleviation capabilities but it does not increase the torsional moment, following the design constraints imposed. The overall alleviation capabilities of the SOF family are reported in Table 2.

Table 2: SOF controllers alleviation capabilities

Controller	SOF003		SOF400		SOF401	
Section	BM	TM	BM	TM	BM	TM
WS00	-0.87%	2.39%	-4.44%	7.40%	-7.59%	30.70%
WS01	-1.43%	2.46%	-6.36%	7.51%	-8.92%	30.65%
WS02	-1.56%	0.81%	-6.78%	1.71%	-9.40%	-0.58%
WS03	-4.45%	0.03%	-14.62%	13.66%	-11.38%	0.00%
WS04	-12.54%	-12.80%	-28.32%	-32.41%	-17.68%	-24.59%

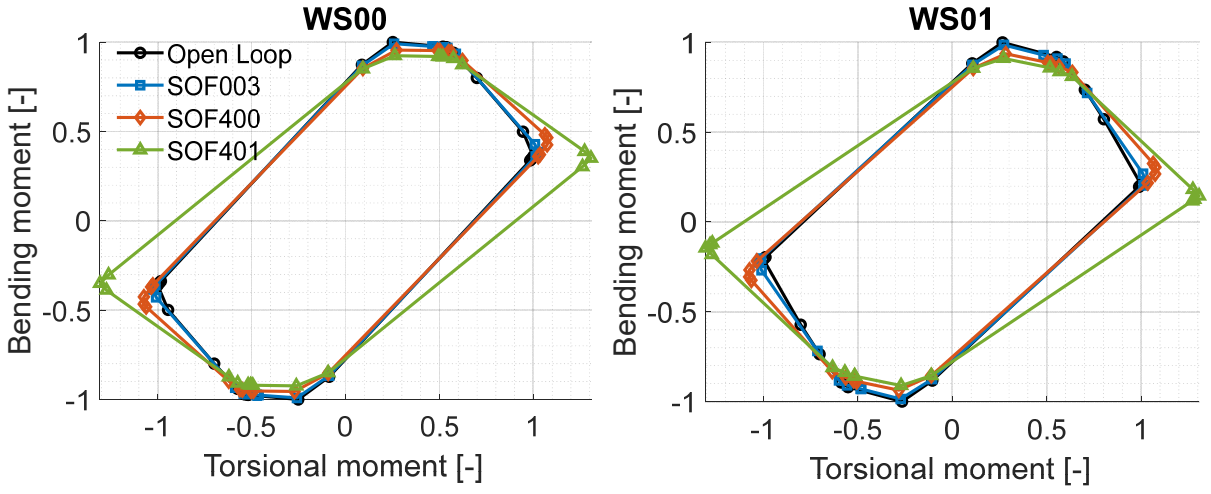

Figure 7: Torque/Bending envelope on the root section and the section before the engine for the SOF controllers

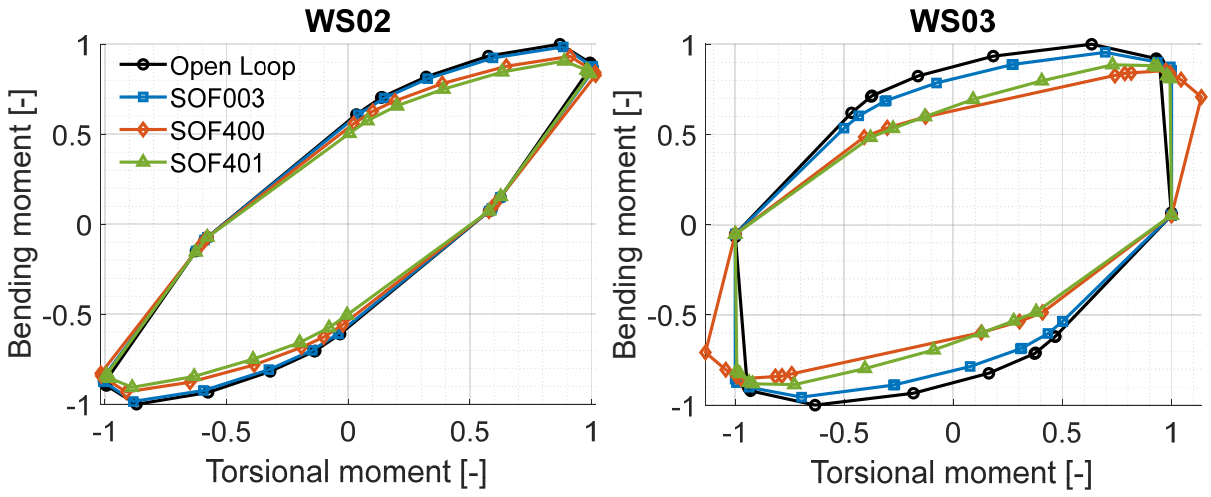

Figure 8: Torque/Bending envelope on the section after the engine and the section before the aileron hinge for the SOF controllers

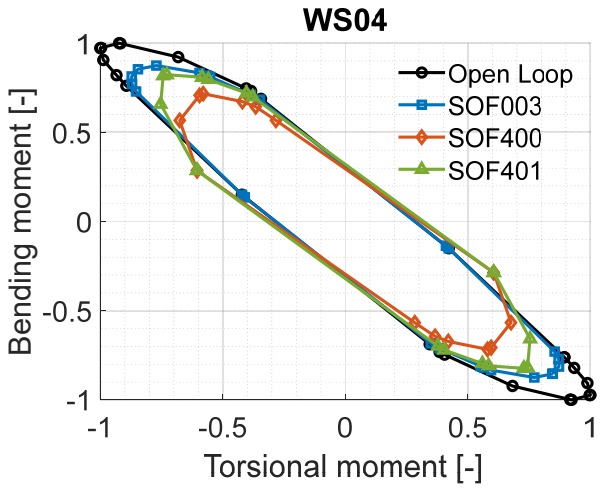

Figure 9: Torque/Bending envelope on the wing tip section for the SOF controllers

The H∞ controller achieved better performances, reducing the root loads of about 15-20% for both bending and torsional moment. The results are obtained with a slightly different simulator, and they are not referred to the entire envelope but only to the most critical gusts for each flight point and mass configuration ad for this reason they are not embedded in previous figures.
The results obtained whit SOF controllers are far from the target reduction (-20%), this is due to the hardware limitations of the FCC to be tested in flight, which are reproduced on the numerical simulator. The sampling rate and controller frequencies (50Hz) imposes to reduce the gain values to maintain the stability of the closed loop system, achieving lower alleviation capabilities. To improve the alleviation capabilities, the sampling rate and the FCC frequencies where increased to 1kHz and the SOF gain matrix was scaled by a uniform factor of 3, $\boldsymbol{G} = 3\boldsymbol{G}_{nominal}$. Table 3 reports the alleviation capabilities of the SOF High Frequency (HF) controllers, while Figure 10 Figure 12 compare the envelope obtained for the nominal controllers (continuous lines) with the HF (dashed lines). In the two cases, the actuators performances are the same, only the electronics hardware performances were numerically modified, and the gain matrix scaled.

Table 3: SOF HF controllers alleviation capabilities

Controller	SOF003HF		SOF400HF		SOF401HF	
Section	BM	TM	BM	TM	BM	TM
WS00	-4.58%	8.04%	-10.64%	7.36%	-17.47%	-9.75%
WS01	-5.50%	8.15%	-12.83%	7.39%	-16.99%	-9.98%
WS02	-5.71%	1.53%	-13.56%	3.85%	-16.96%	-1.49%
WS03	-6.79%	11.70%	-8.65%	32.49%	-12.62%	23.33%
WS04	1.91%	1.89%	25.94%	33.11%	-1.44%	9.69%

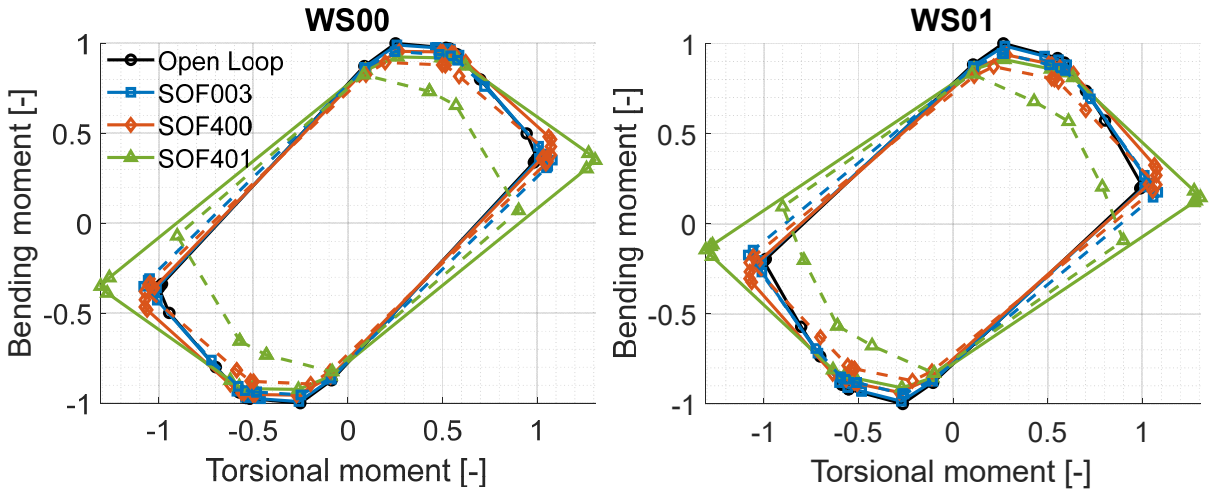

Figure 10: Torque/Bending envelope on the root section and the section before the engine for the SOF HF controllers

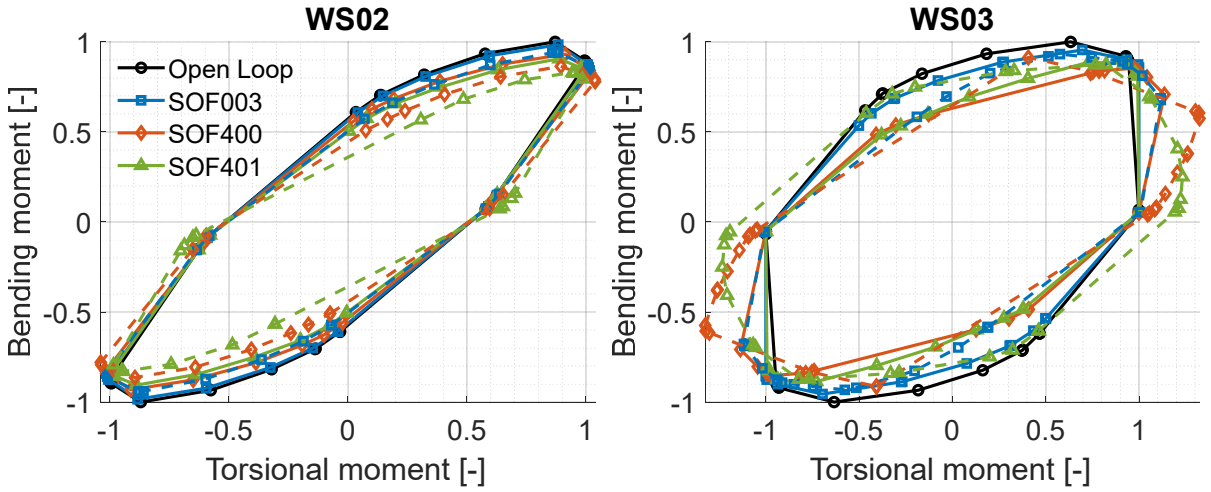

Figure 11: Torque/Bending envelope on the section after the engine and the section before the aileron hinge for the SOF HF controllers

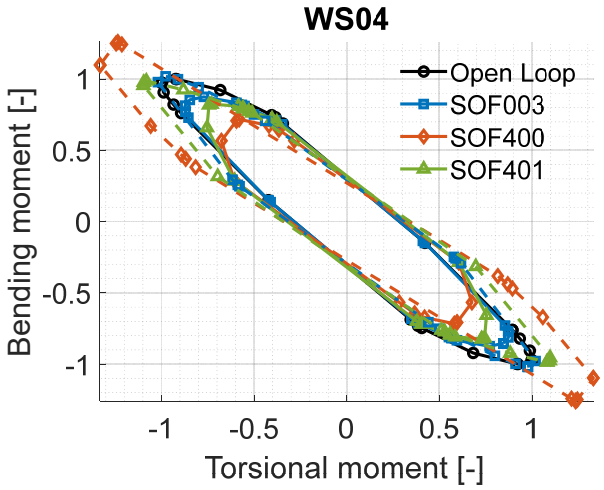

Figure 12: Torque/Bending envelope on the wing tip section for the SOF HF controllers

More aggressive controllers (gain augmentation) have better alleviation capabilities: the SOF HF family reach a 17.47% WRBM reduction with a concurrent WRTM reduction (9.75%), indeed the improved hardware allows a faster response to the gust disturbance. The SOF400 HF (IWT only) reaches an alleviation of 10%, proving the alleviation potential of a small, dedicated control surface located at the wing tip, without the participation of the conventional control surfaces which are used only for the maneuvers. As a drawback, some High Frequency controllers increase the torsional moment spanwise (SOF003HF and SOF400HF) or in the outer part of the wing (SOF401HF). The 20% reduction of the WRBM is slightly missed by the SOF401HF controller, even if it must be considered that this controller is optimized for the nominal hardware and is adapted to the improved (HF) one by simply scaling the gain matrix: a re-tuning of the controller could lead to higher alleviations.
The SOF003 controller was designed considering the concurrent GLA and MLA, in the following the results of a dynamic response to a square wave aileron deflection is reported. As done for the GLA assessment, also in this case the two electronic hardware were considered and considerations like the GLA ones can be drawn. HF controllers better perform but in the outer portion of the wing the torsional moment increases, mainly since in this region the load due to the IWT is introduced to modify the lift distribution and reduce the WRBM. Nominal SOF003 has lower MLA capabilities, and the torsional moment increase is lower but spanwise distributed.

Table 4: SOF003 Maneuver Load Alleviation results

Controller	SOF003		SOF003HF	
Section	BM	TM	BM	TM
WS00	-1.76%	4.04%	-4.52%	-1.66%
WS01	-3.00%	4.63%	-7.43%	-4.17%
WS02	-3.25%	2.55%	-7.67%	7.14%
WS03	-8.08%	12.72%	-15.81%	39.73%
WS04	-21.85%	-17.79%	0.71%	133.80%

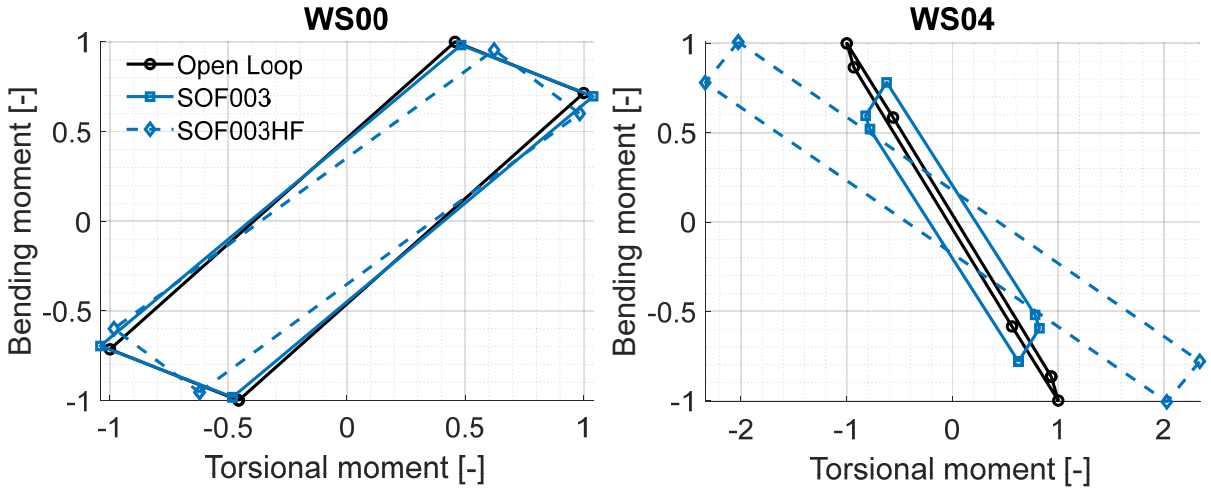

Figure 13: Torque/Bending envelope on the wing root and tip section for the SOF controllers for MLA

6. WIND TUNNEL MODEL

To validate the active control laws developed within the project and to assess their effectiveness, a scaled wind tunnel model was designed and realized. The test facility was the large wing tunnel model available at the Politecnico di Milano (GVPM), it is a closed-circuit wind tunnel with two test rooms: the low turbulence and high-speed test section sizing 4x4x5 m where the airflow reaches 55m/s, and the controlled turbulence low speed test chamber with a section of 12mx4x38m that is located in the return duct. It's scheme is shown in Figure 14.

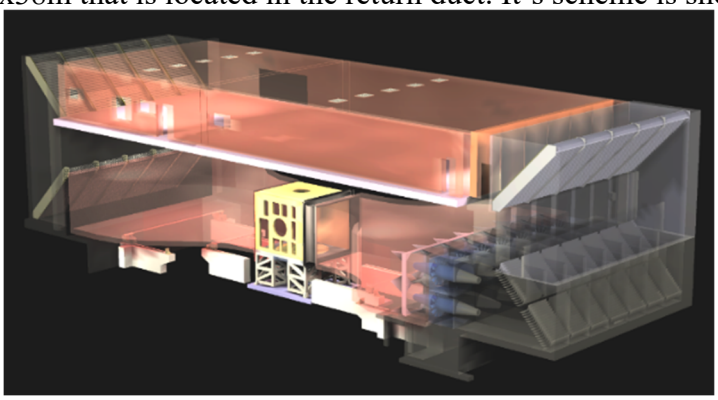

Figure 14: Politecnico di Milano's wind tunnel, in yellow the 4x4x4m high speed test room

The lesson learned with the Clean Sky 1 GLAMOUR project [17][18] were crucial to the development of the WTT3, indeed the philosophy is the same and some components of the GLAMOUR model were recycled and improved for the WTT3 campaign.

The model was scaled considering an iso-frequency approach, such that the time scale of the real aircraft and the scaled model are the same $\lambda_t = \frac{1}{\lambda_f} = 1$. This means that the length and velocity scale must be the same $\lambda_l = \lambda_v$. To fit inside the test room, the length scale is $\lambda_l = \frac{1}{12}$, which would lead to test velocity to low, for this reason a half model configuration was chosen. With this compromise, a length scale becomes $\lambda_l = \frac{1}{6}$ and leads to higher wind tunnel speeds.

Due to installation and accessibility problem, the half model is vertically mounted, the connection between the half fuselage and the wind tunnel floor is realized with a pivot, that preserves the pitch free body motion, mounted on a sledge that preserves the plunge free body motion. Since the gravity acts perpendicularly to the lift, a dedicated Weight Augmentation System (WAS) is used to artificially generate the weight force. The WAS consists in a linear

electric actuator that acts on the moving sledge in correspondence of the centre of gravity of the aircraft, reproducing the weight force indeed.
Once frozen the velocity and length scale, it is possible to find the scale factors to be used to scale the stiffnesses and masses of the real aircraft by keeping constant the ratios between inertial and aerodynamic forces, and the ratio between elastic and aerodynamic forces. The scaling factors used to realize the WTT3 are reported in Table 5.

Table 5: Scaling factor used for the wind tunnel model

Magnitude	Scale factor ($\boldsymbol{\lambda}$)
Length, Velocity	$1/6$
Time, Frequency, reduced frequency	1
Mass	$1/6^3$
Inertia	$1/6^5$
Bending and torsional stiffness	$1/6^6$
Axial stiffness	$1/6^4$

An important ratio which cannot be preserved is the one between the inertial and gravity forces, represented by the Froude number. Thanks to the WAS, it is possible to impose the force that counteracts the lift force, and in the case of unit load factor n=1 it is the weight force. In this way the Froude scaling is preserved only for the plunge motion.
The most sensitive part for the scaling process is the wing, which stiffness properties are reproduced by an aluminium spar on which there are connected in a single point the 3D printed aerodynamic sectors.
Figure 15 (left) shows the installation of the WTT3 model in the test room: a dummy floor covers the WAS-sledge-pivot connection to the room's floor and the gust generator is mounted at the inlet of the test section. Figure 15 (right) represents the structural skeleton of the aeroelastic model, highlighting the WAS-sledge-pivot mechanism.

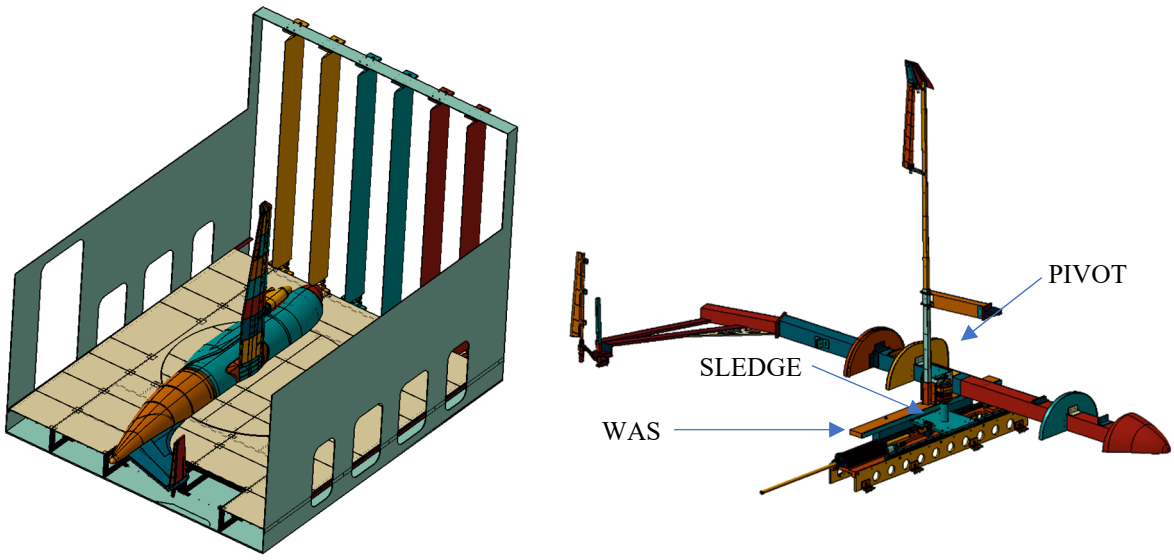

Figure 15: (left) WTT3 WT model in test condition with the gust generator at the inlet of the test room, (right) WTT3 structural model

Figure 16: The final assembled wing with an internal view of the nacelle and the IWT installed

Figure 17: The complete WWT3 model installed in the Large POLIMI's wind tunnel test chamber

The gust generator consists in 6 vanes [55] that are simultaneously deflected to generate the desired gust shape. The comparison between the numerical scaled gust and the one obtained in the wind tunnel is illustrated in Figure 18, which shows how the 1-cos shape is obtained and the peak value is reached, a slight difference is present in terms of frequency.

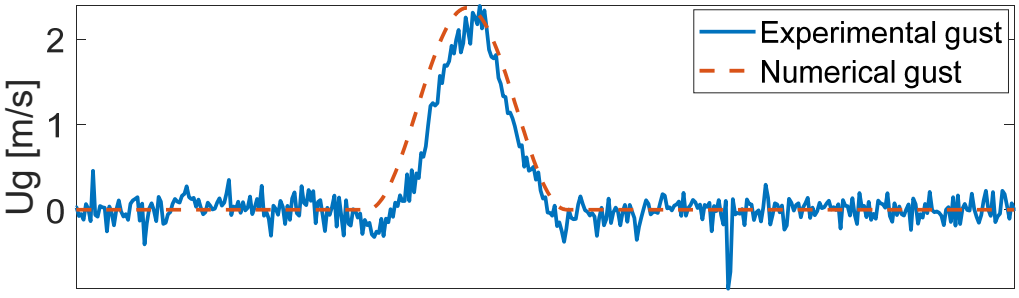

Figure 18: Experimental and numerical gust profile

The model is equipped with movable surfaces (aileron, IWT flap and elevator) commanded by a Harmonic-Drive servo-motor [56][57] used to trim the aircraft (elevator only) and to perform the GLA. The model is equipped with many sensors which are used to monitor the test and to provide the control feedback: accelerometers located in the wings, fuselage and tail planes, strain gages along the wing spar, encoder to measure the pitch and control surfaces rotations, a

potentiometer to measure the plunge. Some accelerometers are located in the same position of the acceleration sensors used to design the control laws, e.g. the ones on the CoG, on the wing tip and on the engine section.
Two gust frequencies were considered in the tests, both with positive e negative amplitudes, they are the gust tuned on the 1st wing bending moment and the gust producing the highest Wing Root Bending Moment (WRBM).
The comparison between the numerical and experimental results shows how the aeroelastic behaviour of the WT model is well predicted by its numerical model, Figure 19 compares the acceleration obtained with the numerical model (scaled reference aircraft) and the one measured in the wind tunnel for a gust excitation without any GLA controller (open-loop); the peak value is well matched by the numerical prediction but the numerical response appears to be more damped.

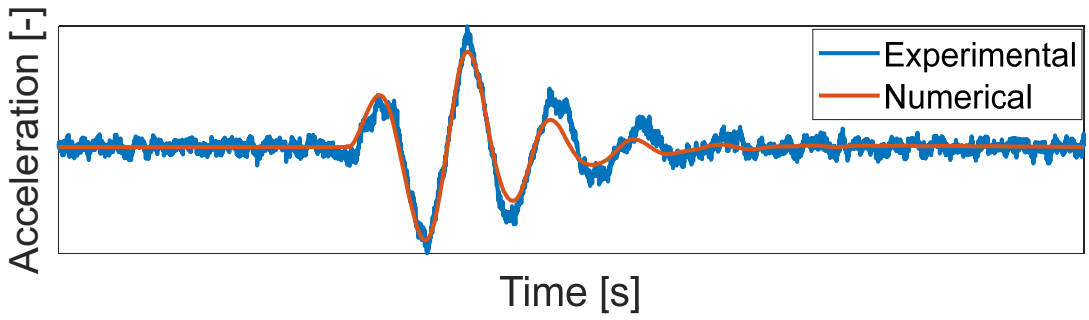

Figure 19: Comparison of the wing tip acceleration experimentally measured and numerically obtained

Figure 20 shows the evolution of the WRBM, the 1st peak value is perfectly matched by the numerical model, but as in the case of the acceleration, the evolution of the numerical WRBM is more damped.

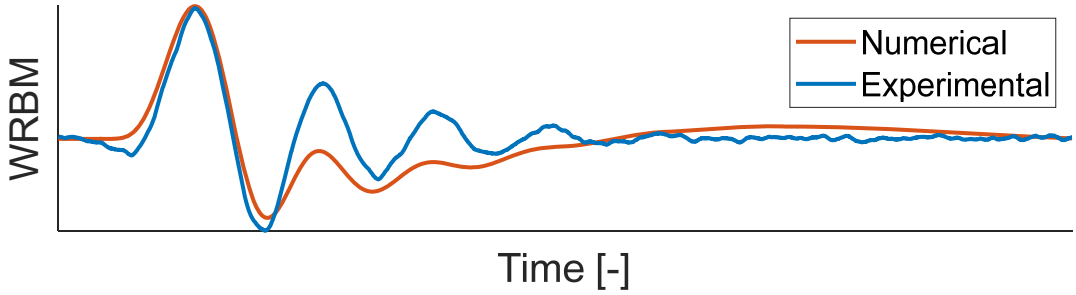

Figure 20: Comparison of the WRBM experimentally measured and numerically obtained

These first results provide an indication: the free body motion is not perfectly reproduced; this can be noted by the absence of the free body response after the first peak.

7. WIND TUNNEL TEST RESULTS

The wind tunnel test campaign aimed to investigate the behavior of the GLA control laws on the scaled model, two flight conditions were investigated, and they are the maximum operating speed and dive speed at the corner point. The WT speed considered are the reference EAS values scaled by $\lambda_v = \frac{1}{6}$. The gust amplitude considered are obtained by scaling the $V_{gust(EAS)}$ of the same scale factor. The gust frequencies tested are the one tuned on the first bending mode and the one producing the maximum WRBM. This provides the test matrix reported in Table 6 repeated for each controller both in open and closed loop condition, for a total of 16 points for each controller.

Table 6: Test matrix

Flight Point	Gust Frequencies	Amplitude
VMO	Tuned & WRBM max	±Tuned & ±WRBM max
VD	Tuned & WRBM max	±Tuned & ±WRBM max

Figure 21 shows the comparison between the Open and Closed, experimental and numerical WRBM. It is possible to see how the peak value of the gust is matched but the response is different after it: the WT model behaves more like a clamped wing where the rigid body response is missing. This aspect directly impacts on the controllers' performances where the CoG acceleration is a feedback measure used to compute the control surfaces deflection, in the SOF case if the CoG acceleration is value, the required deflection is lower due to the proportional nature of the controller. This latest aspect can be seen in Figure 22, where the experimental results are compared with the numerical ones: a generalized lack of correlation is present for several reasons:

- The rigid body motion is not fully reproduced, and it introduces two main issues: the first one is the missing CoG acceleration in the feedback which limits the surface command with respect the numerical prediction, the second one is the "clamped" behavior of the model where is missing the load relief due to the plunge motion. While the second effect affects both OL and CL responses, the first one impact on the CL response only. This aspect strongly influenced the H∞ controller because the rigid body measures were relevant for the state reconstruction and for the input computation.
- The model is trimmed with the WAS, but due to the lift force the pitch limiter device introduces a static friction that makes difficult to trim the model with the elevator. This is the reason why the model is not fully free in plunge motion. This is translated into an uncertainty in the initial trim condition which may leads to different gust responses.
- The efficiency of the control surface is lower in the wind tunnel model and higher deflection are required to obtain the same responses, as explained in the following.

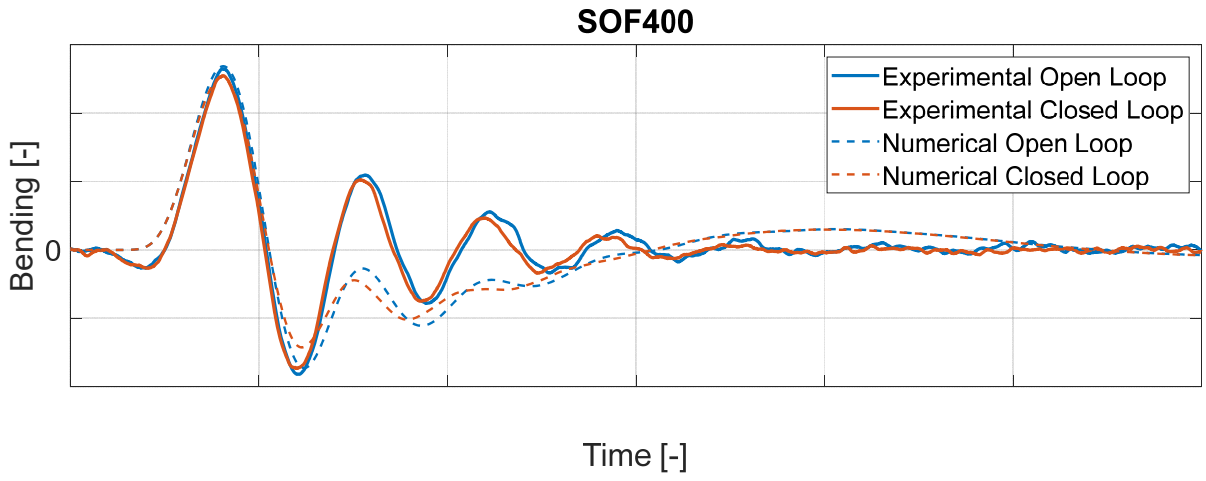

Figure 21: Numerical vs. Experimental Open and Closed loop at WS00 for SOF400

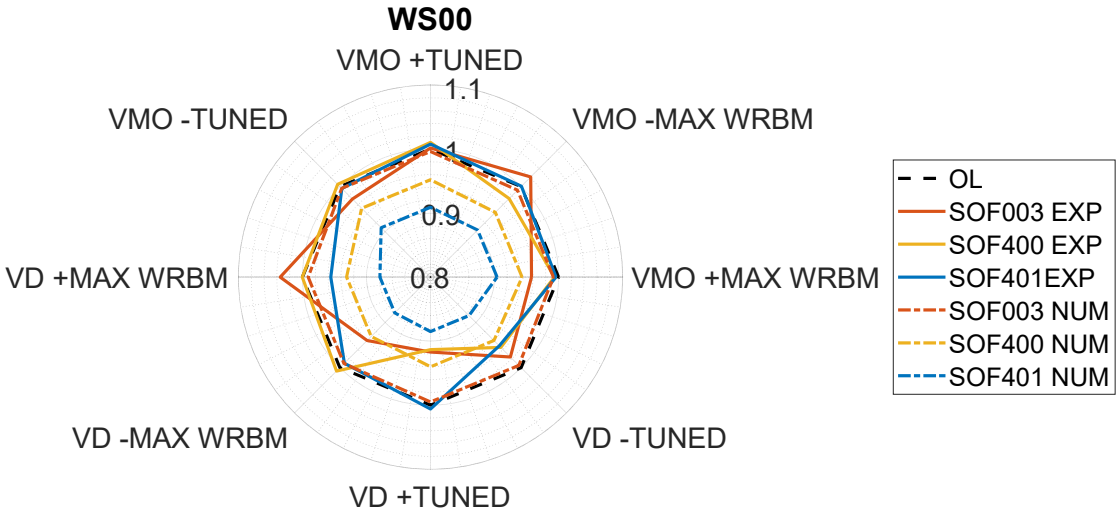

Figure 22: WRBM variation for SOF controller, experimental and numerical results

A comparison between the numerical and experimental transfer functions between the aileron rotation and the wing tip acceleration (Figure 23), shows a lower magnitude for the WT model, this fact is due to the lower aerodynamic efficiency of the control surfaces in low-speed condition. This can be partially solved in the wind-tunnel by scaling the control input by a constant ratio, with a kind of amplifier (gain value in the WT Simulink control scheme). The drawback is that excessive scaling factor may lead to saturation in speed and velocity affecting the test with a non-linear effects, for this reason instead of a scaling factor of $\frac{1}{0.6} = 1.\overline{6}$ it was used a factor of $\frac{1}{0.75} = 1.\overline{3}$ that proved to do not reach saturation in the numerical simulation of the SOF HF family. This partially recover the control surfaces effectiveness loss.

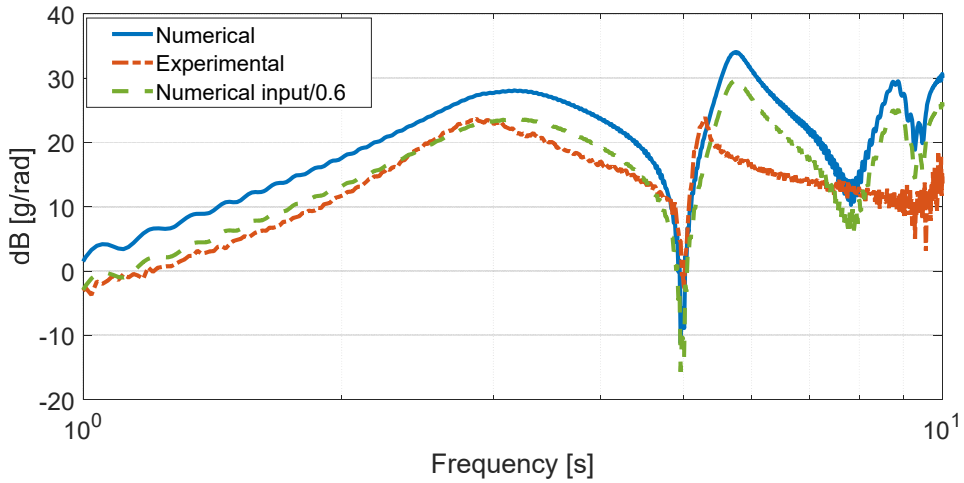

Figure 23: Experimental FrF comparison

Figure 24 sows the results obtained with the augmented experimental and numerical gains, the comparison is performed between the numerical simulation obtained for the SOF HF family, where better electronics allows to scale the nominal matrix by a factor of 3. The experiment test used a scale factor of 4 which considers the gain scaling and the 0.75 factor due to the control surfaces efficiency loss. In this case better alleviation performance can be achieved w.r.t. the nominal gains, but the experiment is still affected by the limitations due to the limited plunge as discussed before. However, a WRBM reduction of 20% is achieved for the experimental SOF401 HF controller.

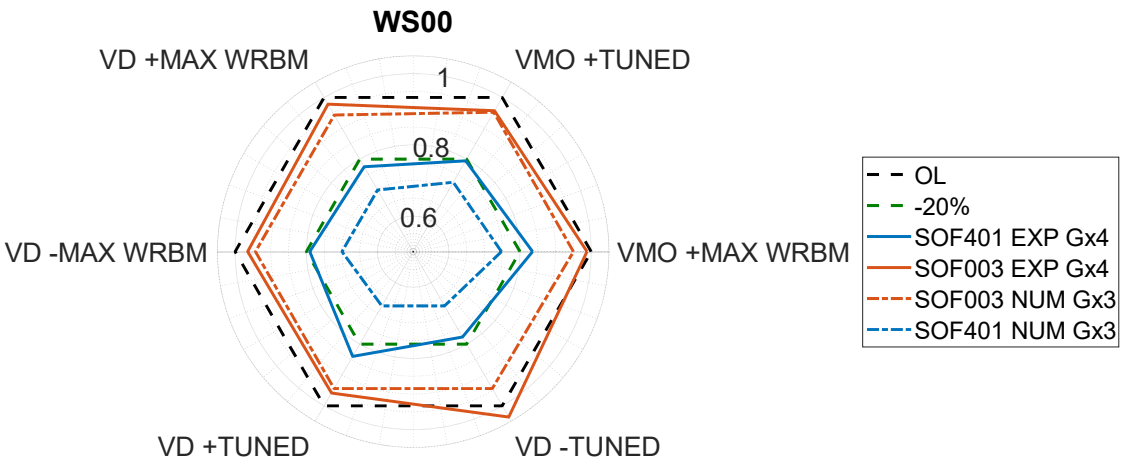

Figure 24: WRBM variation for SOF controller with augmented gains, experimental and numerical results

8. LESSON LEARNED AND EXTENSION TO THE REAL AIRCRAFT

The AIRGREEN2 project produced a huge number of results and extended the knowledge about the Gust Load Alleviation technologies for a new generation regional liner. This work shows how new dedicated control surfaces can be used to perform GLA in combination with conventional control surfaces or as dedicated surfaces. Key factor for the effectiveness of the control laws is an adequate hardware, which must ensure sufficient performances to achieve reduction close to the target of 20% of the dynamic loads.

The designed Wind Tunnel model allowed to perform an extensive validation campaign of the developed GLA controller, remarking their effectiveness and their robustness.

With respect to the previous GLAMOUR project [17][18], some hardware modification improved the repeatability of the test, hence providing more reliable results. Despite this improvement, the rigid body motion of the model is not fully reproduced and impact directly on the effectiveness of the controllers. At the end of the test session, a gust response without the pitch limiter mounted show a sensible improvement of the model trimming (pitch motion), while other modifications are now under implementation to better reproduce the plunge motion.

9. AKNOWLEDGEMENTS

Part of the research described in this document has been carried out in the framework of AIRGREEN2 Project, which gratefully received funding from the Clean Sky 2 Joint Undertaking, under the European's Union Horizon 2020 research and innovation Program, Grant Agreement No. 807089-REG. A special thanks to Prof. Paolo Mantegazza for his continuous support.

10. REFERENCES

[1] Harpur, N. F. "The effect of active control systems on structural design criteria." AGARD Active Control Systems for Load Alleviation, Flutter Suppression and Ride Control p 11-22(SEE N 74-25550 15-02) (1974).

[2] Regan, Christopher D., and Christine V. Jutte. "Survey of applications of active control technology for gust alleviation and new challenges for lighter-weight aircraft". No. DFRC-E-DAA-TN4736. 2012.

[3] McLean, D. "Gust-alleviation control systems for aircraft." Proceedings of the Institution of Electrical Engineers. Vol. 125. No. 7. IET Digital Library, 1978.

[4] W. H. Phillips, “Gust alleviation,” in Performance, dynamics, and design of aeronautical and space vehicles, pp. 505–553, NASA-SP-258, L-6892, 1971.
[5] Lock, Wilton P., et al. “Flight investigation of a structural mode control system for the XB-70 aircraft”. No. NASA-TN-D-7420. 1973.
[6] Wykes, John H., Louis U. Nardi, and Alva S. Mori. “XB-70 structural mode control system design and performance analyses”. National Aeronautics and Space Administration, 1970.
[7] Burris, P. M., and M. A. Bender. “Aircraft load alleviation and mode stabilization (LAMS): B-52 system analysis, synthesis, and design”. Boeing Wichita Co., 1969.
[8] Johnston, J. F. “Accelerated development and flight evaluation of active controls concepts for subsonic transport aircraft”. Volume 1: Load alleviation/extended span development and flight tests. No. NASA-CR-159097. 1979.
[9] Britt, R. T., et al. “Aeroservoelastic characteristics of the B-2 bomber and implications for future large aircraft”. Northrop Grumman Corp Pico Rivera Ca Military Aircraft Systems Div, 2000.
[10] Karpel, M., Shousterman, A., Climent, H., & Reyes, M. (2013). “Dynamic response to wake encounter”. In 54th AIAA/ASME/ASCE/AHS/ASC Structures, Structural Dynamics, and Materials Conference (p. 1921).
[11] Hesse, H., & Palacios, R. (2016). “Dynamic load alleviation in wake vortex encounters”. Journal of Guidance, Control, and Dynamics, 39(4), 801-813.
[12] Y. Matsuzaki, T. Ueda, T. Miyazawa, and H. Matsushita, “Wind tunnel test and analysis on gust load alleviation of a transport-type wing,” in 87-0781. 28th Structures, Structural Dynamics and Materials Conference, 1987.
[13] Y. Matsuzaki, T. Ueda, Y. Miyazawa, and H. Matsushita, “Gust load alleviation of a transport-type wing- test and analysis,” Journal of aircraft, vol. 26, no. 4, pp. 322–327, 1989.
[14] J. C. Yeager, “Implementation and Testing of Turbulence Models for the F18-HARV Simulation,” Lockheed Martin Engineering & Sciences, NASA CR-1998-206937, 1998.
[15] A. De Gaspari, S. Ricci, L. Riccobene, and A. Scotti, “Active aeroelastic control over a multisurface wing: Modeling and wind-tunnel testing,” AIAA journal, vol. 47, no. 9, pp. 1995–2010, 2009.
[16] S. Ricci and A. Scotti, “Wind tunnel testing of an active controlled wing under gust excitation,” in Proceedings of the 49th AIAA/ASME/ASCE/AHS/ASC structures, structural dynamics, and materials conference, Schaumburg, IL, USA, pp. 7–10, 2008.
[17] Ricci, Sergio, et al. “Design and wind tunnel test validation of gust load alleviation systems”. 58th AIAA/ASCE/AHS/ASC Structures, Structural Dynamics, and Materials Conference. 2017.
[18] Ricci, Sergio, et al. “Wind tunnel experimental validation of future green regional a/c gust load alleviation control system.” International Forum on Aeroelasticity and Structural Dynamics (IFASD 2015). 2015.
[19] R. C. Scott, T. Allen, M. Castelluccio, B. Sexton, S. Claggett, J. R. Dykman, C. Funk, D. Coulson, and R. E. Bartels, “Aeroservoelastic wind-tunnel test of the sugar truss braced wing wind-tunnel model,” in 56th AIAA/ASCE/AHS/ASC Structures, Structural Dynamics, and Materials Conference. AIAA SciTech Forum, 2015.
[20] K. Shao, Z.Wu, C. Yang, L. Chen, and B. Lv, “Design of an adaptive gust response alleviation control system: simulations and experiments,” Journal of Aircraft, vol. 47, no. 3, p. 1022, 2010.
[21] W. A. Silva, P. Boyd, J. R. Florance, M. D. Sanetrik, C. D. Wieseman, W. L. Stevens, C. J. Funk, J. Hur, D. M. Christhilf, and D. A. Coulson, “An overview of preliminary computational and experimental results for the semi-span super-sonic transport (s4t) wind-tunnel model,” in International Forum on Aeroelasticity and Structural Dynamics, vol. IFASD-2011-147, 2011.

[22] B. Moulin, E. Ritz, P. C. Chen, D. H. Lee, , and Z. Zhang, “Cfd-based control for flutter suppression, gust load alleviation, and ride quality enhancement for the S4T model,” in 51st AIAA/ASME/ASCE/AHS/ASC Structures, Structural Dynamics, and Materials Conference 18th 12 - 15 April 2010, Orlando, Florida, 2010.

[23] C. Poussot-Vassal, F. Demourant, A. Lepage, and D. Le Bihan, “Gust load alleviation: Identification, control, and wind tunnel testing of a 2-d aeroelastic airfoil,” IEEE Transactions on Control Systems Technology, 2016.

[24] H.-G. Giesseler and G. Beuck, “Design procedure for an active load alleviation system (las) for a modern ransport aircraft,” in Congress of the International Council of the Aeronautical Sciences (ICAS), Toulouse, Fr (1984), 1984.

[25] I. Abel, R. V. Doggett, J. R. Newsom, and M. Sandford, “Dynamic wind-tunnel testing’ of active controls by the nasa langley research center,” in Agard No.262 Ground And Flight Testing For Aircraft Guidance And Control, 1985.

[26] E. Vartio, A. Shimko, C. P. Tilmann, and P. M. Flick, “Structural modal control and gust load alleviation for a sensorcraft concept,” in Proceedings of the 46th AIAA/ASME/ASCE/AHS/ASC Structures, Structural Dynamics & Materials Conference, Austin, TX, USA, pp. 18–21, 2005.

[27] K. B. Penning, P. S. Zink, P.Wei, A. P. De La Garza, M. H. Love, and J. Martinez, “GLA and flutter suppression for a sensorcraft class concept using system identification,” in 26th AIAA Applied Aerodynamic Conference, AIAA-2008-7188, pp. 1–13, 2008.

[28] R. C. Scott, T. K. Vetter, K. B. Penning, D. A. Coulson, and J. Heeg, “Aeroservoelastic testing of a sidewall mounted free flying wind-tunnel model,” in 26th AIAA Applied Aerodynamics Conference. 18-21 August 2008. Honolulu, Hawaii, USA, vol. AIAA 2008-7186, 2008.

[29] R. C. Scott, M. A. Castelluccio, D. A. Coulson, and J. Heeg, “Aeroservoelastic wind-tunnel tests of a freeflying, joined-wing sensorcraft model for gust load alleviation,” in 52nd AIAA/ASME/ASCE/AHS/ASC Structures, Structural Dynamics and Materials Conference. 4 - 7 April 2011, Denver, Colorado, 2011.

[30] S. I. Kuzmina, F. Ishmuratov, M. Zichenkov, and V. Chedrik, “Integrated numerical and experimental investigations of the active/passive aeroelastic concepts on the european research aeroelastic model (euram),” Journal of Aeroelasticity and Structural Dynamics, vol. 2, no. 2, pp. 31–51, 2011.

[31] S. Kuzmina, G. Amiryants, J. Schweiger, J. Cooper, M. Amprikidis, and O. Sensberg, “Review and outlook on active and passive aeroelastic design concept for future aircraft,” in 23rd International Congress Of Aeronautical Sciences (ICAS). 8-13 September, 2002, Toronto, Canada, vol. ICAS 2002-4.3.2, 2002.

[32] Ameduri, S., Amoroso, F., Carossa, G. M., Concilio, A., Dimino, I., Giuliani, M., ... & Romano, F.. “An Overview of the AG2 Project: Latest Achievements”. In AIAA Scitech 2022 Forum (p. 0717)., 2022

[33] Dimino, I., Moens, F., Pecora, R., De Gaspari, A., Ricci, S., Ameduri, S., ... & Carossa, G. M.. “Morphing Wing Technologies within the Airgreen 2 Project”. In AIAA Scitech 2022 Forum (p. 0718)., 2022

[34] De Gaspari, A. “Multiobjective Optimization for the Aero-Structural Design of Adaptive Compliant Wing Devices”. Applied Sciences, 10(18), 6380, 2020

[35] Cavalieri, V., De Gaspari, A., & Ricci, S.. “Optimization of compliant adaptive structures in the design of a morphing droop nose”. Smart Materials and Structures, 29(7), 075020, 2020

[36] De Gaspari, A., Cavalieri, V., & Ricci, S.. “Advanced design of a full-scale active morphing droop nose”. International Journal of Aerospace Engineering, 2020.

[37] De Gaspari, A., & Moens, F.. $Aerodynamic shape design and validation of an advanced high-lift device for a regional aircraft with morphing droop nose$. International Journal of Aerospace Engineering, 2019.

[38] De Gaspari, A., Gilardelli, A., Ricci, S., Airoldi, A., & Moens, F.. "Design of a leading edge morphing based on compliant structures in the framework of the CS2-AirGreen2 project". In Smart Materials, Adaptive Structures and Intelligent Systems (Vol. 51944, p. V001T04A025). American Society of Mechanical Engineers., 2018

[39] Ricci, S., De Gaspari, A., Gilardelli, A., & Airoldi, A. "Design of a leading edge morphing based on compliant structures for a twin-prop regional aircraft". In 2018 AIAA/AHS adaptive structures conference (p. 1063).

[40] Pecora, R. "Integrated design approaches for an innovative multifunctional flap architecture based on distributed electromechanical actuation". In AIAA SCITECH 2022 Forum (p. 0719).

[41] Fonte, Federico, Francesco Toffol, and Sergio Ricci. "Design of a wing tip device for active maneuver and gust load alleviation." 2018 AIAA/ASCE/AHS/ASC Structures, Structural Dynamics, and Materials Conference.

[42] Toffol, Francesco, Federico Fonte, and Sergio Ricci. "Design of an innovative wing tip device." 17th International Forum on Aeroelasticity and Structural Dynamics (IFASD 2017)..

[43] Ripepi, M., & Mantegazza, P. (2013). "Improved matrix fraction approximation of aerodynamic transfer matrices". AIAA journal, 51(5), 1156-1173.

[44] Cavagna, Luca, Sergio Ricci, and Lorenzo Travaglini. "NeoCASS: an integrated tool for structural sizing, aeroelastic analysis and MDO at conceptual design level." Progress in Aerospace Sciences 47.8 (2011): 621-635.

[45] Cavagna, L., De Gaspari, A., Ricci, S., Riccobene, L., & Travaglini, L. (2012). "Neocass: an Open Source Environment for the Aeroelastic Analysis at Conceptual Design Level". Brisbane, Australia.

[46] Cavagna, L., Ricci, S., & Riccobene, L. . "NeoCASS, a tool for aeroelastic optimization at aircraft conceptual design level". In International Forum on Aeroelasticity and Structural Dynamics (IFASD 2009) (pp. 1-15).

[47] Syrmos, V., Abdallah, C., Dorato, P., and Grigoriadis, K., "Static output feedback—A survey," Automatica, Vol. 33, No. 2, 1997, pp. 125–137. https://doi.org/10.1016/S0005-1098(96)00141-0.

[48] Ghiringhelli, G. L., Lanz, M., and Mantegazza, P., "Active flutter suppression for a wing model," Journal of Aircraft, Vol. 27, No. 4, 1990, pp. 334–341. https://doi.org/10.2514/3.25277.

[49] Ghiringhelli, G. L., Lanz, M., Mantegazza, P., and Ricci, S., "Active Flutter Suppression Techniques in Aircraft Wings" Control and Dynamic Systems, Vol. 92, 1992, pp. 57–115. https://doi.org/10.1016/B978-0-12-012752-8.50007-6.

[50] Fonte, F., Ricci, S., and Mantegazza, P., "Gust load alleviation for a regional aircraft through a static output feedback" Journal of Aircraft, Vol. 52, No. 5, 2015, pp. 1559–1574. https://doi.org/10.2514/1.C032995.

[51] Skogestad, S., and Postlethwaite, I., "Multivariable feedback control: analysis and design", 2nd ed., Wiley-Interscience, 2005.

[52] Choi, H. H., & Chung, M. J. (1997). "An LMI approach to H∞ controller design for linear time-delay systems". Automatica, 33(4), 737-739.

[53] Kalman, R. E. (1960, August). "On the general theory of control systems". In Proceedings First International Conference on Automatic Control, Moscow, USSR (pp. 481-492).

[54] Stoica, A. (1997, July). “Optimal H-infinity design of a control system for the angle of attack”. In 1997 European Control Conference (ECC) (pp. 337-342). IEEE.
[55] Fonte, F., Riccobene, L., Ricci, S., Adden, S., & Martegani, M. (2016, September). “Design, manufacturing and validation of a gust generator for wind tunnel test of a large scale aeroelastic model”. In 30th Congress of the International Council of the Aeronautical Science, Daejeon (pp. 25-30).
[56] De Gaspari, A., Mannarino, A., and Mantegazza, P., “A dual loop strategy for the design of a control surface actuation system with nonlinear limitations”, Mechanical Systems and Signal Processing, 90(2017):334–349, 2017, doi: 10.1016/j.ymssp.2016.12.037
[57] De Gaspari, A. and Mantegazza, P., “Dual loop servo positioning using PI(n+m) controller”, Submitted to Mechanical Systems and Signal Processing.

11. COPYRIGHT STATEMENT